IEEE Access
Multidisciplinary | Rapid Review | Open Access Journal

Received February 25, 2020, accepted March 8, 2020, date of publication April 6, 2020, date of current version April 21, 2020.

Digital Object Identifier 10.1109/ACCESS.2020.2985721

Modeling and Analysis of the Load Torque Acting on the Drilling Fluid Continuous Wave Generator

JIAFENG WU, BOTAO ZHOU, NING HAN, JIANMING JIANG, SHUXING ZHAO, DONGLI QIN, AND RUIHE WANG

[1]Key Laboratory of Unconventional Oil and Gas Development, Ministry of Education, China University of Petroleum (East China), Qingdao 266580, China
[2]School of Petroleum Engineering, China University of Petroleum (East China), Qingdao 266580, China

Corresponding author: Jiafeng Wu (wujiafeng@upc.edu.cn)

This work was supported in part by the National Natural Science Foundation of China under Grant 51604296, in part by the Fundamental Research Funds for the Central Universities under Grant 19CX02066A, in part by the Key Research and Development Program of Shandong Province under Grant 2019GHZ001, and in part by the Scientific Research Foundation of the China University of Petroleum under Grant YJ201601085.

ABSTRACT Drilling fluid continuous wave(DFCW) generator is an advanced downhole instrument and has broad application prospects. The load torque acting on the DFCW generator has a great impact on the performance on the DFCW generator, and there is a lack of theory describing the load torque because of the irregularity of the rotary valve. In this paper, the drilling fluid flow area is divided into the curve flow area, the radial flow area and the axial flow area. The flow area of each part is divided into several meshes based on finite element theory, then the load torque acting on each part is calculated based on the fluid momentum conservation theory. The theoretical model is verified by combining the simulation and the experiment, and the effects of the discharge and the axial gap on the load torque are analyzed. The research results show that:(1) the theoretical model can be used to determine the load torque, (2) the amplitude of the load torque reduces as the gap decreases and increases rapidly as the discharge increases. The results can provide the theoretical guidance for the structure design of the rotary valve and the control system design of the drilling fluid continuous wave generator.

INDEX TERMS Load torque, irregular orifice, drilling fluid continuous wave, CFD.

I. INTRODUCTION

In the automatic drilling stage, it is necessary to transmit downhole information to the surface quickly and in real time, which makes the downhole information transmission technology important [1]. As an advanced downhole information transmission technology, drilling fluid continuous wave (DFCW) technology has a broad application prospect due to its good robustness, high transmission speed and good quality of the signal [1]–[16].

DFCW generator is the key mechatronic instrument to generate DFCW. It is mainly composed of a rotary valve and a driven system. The rotary valve contains a pair of stator and rotor, and there is a gap between the stator and rotor. When it works, the rotary valve rotates in the driven by the driven system, and periodically blocks the flow path of the drilling fluid. Then the DFCW will generate upstream of the rotary valve and carries the downhole information to the ground [7]–[17]. Due to the impact of the high pressure and high-speed drilling fluid, there will be a great load torque acting on the rotary valve, which will cause high energy cost and improve the difficulty on the control of the DFCW [11], [15]. Therefore, it is necessary to analyze the load torque acting on the rotary valve and its influence factors.

There is a few research on the influence of the flow torque acting on the rotary valve [18], [19]. Wang *et al.* [19] proposed a theoretical model for hydraulic torque acting on rotary directional control valve based on fluid momentum theorem, but the orifice of the rotary valve is simple rectangular. In the drilling engineering, the rotary valve used in the DFCW generator has the irregular orifice. It will cause that the flow direction of the drilling fluid is not the same along the curve of the valve port, at the same time, when the rotary valve rotates, the flow direction of the drilling fluid also changes. Due to the existence of the gap, some fluid flows in the gap, which will also influence the flow direction. Thus, the calculation method is not applicable. Yan *et al.* [13] designed the rotary valve and analysis the torque acting on the

The associate editor coordinating the review of this manuscript and approving it for publication was Wen-Sheng Zhao.

rotary valve via CFD, but there is a lack of the method using to calculate the torque and it is not convenient to be used in other situation. Therefore, it is necessary to describe the load torque acting on the rotary valve of the DFCW generator in theory.

Most of the related studies are aimed at the hydraulic force acting on the slide valve [20], [21]. For the valves with simple flow-path shape, the fluid momentum conservation theory is often used to solve the load force problems because the velocity vector and fluid mass through the simple valve are easily calculated. And in many cases, CFD is used for analysis [22]–[25]. However, 3D fluid dynamics analysis will cost a large amount of computation time and storage space, and it is difficult to describe the influence laws of various factors on the flow torque accurately.

In summary, the related researches are about the load torque acting on the sliding valve and the load torque acting on the rotary valve with the simple orifices. But the orifice shape of the common valve is three-dimensional irregular. In this paper, a mathematical model for the load torque acting on the DFCW generator will be established based on the fluid momentum theorem and the finite element method. In addition, the influence of structural parameters of the DFCW generator and drilling parameters on load torque will be studied. The structure of this paper are as follows: In section II, the mathematical model will be established and in section III and IV, the CFD simulation and experiment are used to verify the correctness of the theory model. Then the influencing factors and laws will be discussed.

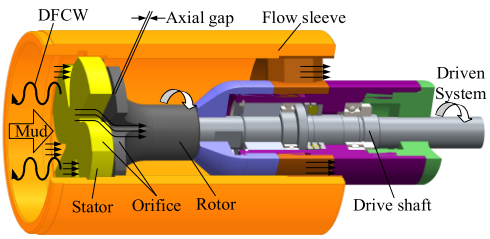

FIGURE 1. Local structure of the DFCW generator.

II. MODELING

A. SYSTEM DESCRIPTION

The local structure of the DFCW generator is shown in Fig.1. The DFCW generator mainly contains the rotary valve, the driven system and the drive shaft. The rotary valve is composed of a stator and a rotor, and there is an axial gap between the stator and the rotor. When the DFCW generator works, the drilling fluid flows through the stator, gap and rotor. With the continuous rotation of the rotor, the flow path of the drilling fluid is periodically blocked, and the DFCW generates in the upstream of the rotary valve. To increase the transmission quality of the downhole information, the DFCW is often needed to be sinusoidal. And according to the previous research, it is possible to generator sinusoidal DFCW when the stator and rotor have the same shape [7]. The load torque acting on the rotary valve consists of the hydraulic torque acting on the rotary valve and the system friction torque, which is produced by the mechanical structure. The amplitude of hydraulic torque is much larger than that of the friction torque, and it will affect the performance of the DFCW generator obviously.

B. THE STRUCTURE OF THE ROTARY VALVE

In this section, the rotary valve with known orifice curve is designed to produce the sinusoidal DFCW. On the assumption of constant pressure generated at the outlet of the rotary valve and the influence of the axial clearance and the radial clearance considered, the rotary valve is designed and studied [7]. When the rotary valve rotates at a constant speed, the sinusoidal DFCW can be generated at the inlet of the rotary valve. The valve opening can be expressed as [7]:

$$\tau(t) = [1 + 4CC_d^2A_o^2\cos^2\frac{N\omega t}{2}/(\rho Q^2)]^{-\frac{1}{2}} \tag{1}$$

where C is the DFCW amplitude. C_d is the flow coefficient in rotary valve. A_0 is the maximum flow area of the rotary valve orifice. N is the Number of blades of the rotary valve. ω is the rotating speed of rotary valve. t is the time. ρ is the drilling fluid density. Q is the pump flow.

The orifice curves can be defined in the polar coordinate system. $r(\theta)$ is the polar radius of the valve orifices and denotes the distance from the axial line to the intersection point between the orifice curves of the stator and the rotor where $\theta \in [0, \frac{\pi}{N}]$. And it can be expressed as [7]:

$$r(\theta) = -\zeta\lambda s + \sqrt{(\zeta\lambda s)^2 + R^2 - \frac{kA_o\sin(N\theta)}{[k\cos(N\theta) + k + 1]^{1.5}}} \tag{2}$$

where $\zeta = 1 - \int_0^1 r[(\frac{\pi}{N} - \theta)x + \theta]/r(\theta)dx$ is a correction coefficient that can be used to correct for the influence of the axial clearance s on the whole flow area. $k = \frac{C}{P_o} = \frac{2CC_d^2A_o^2}{\rho Q^2}$ is the relative intensity. R is the outer diameter of the rotor. s is the axial clearance between the stator and rotor. θ is the rotation angle of the rotor. r is the polar radius. λ is the coefficient.

The length L of the orifice curves can be obtained as [7]:

$$L = \int_0^{\frac{\pi}{N}} r(\theta)d\theta \tag{3}$$

According to the method, the structure of the rotary valve can be determined. Then the load torque can be calculated based on the structure.

C. THE LOAD TORQUE COMBINATION MODEL

Because the hydraulic torque has a more significant impact on the performance of the continuous wave generator, in this section, the hydraulic torque will be modeled and analyzed. There are some assumptions: the fluid is incompressible, the fluid is not lost in the valve and the fluid property is constant. Based on the fluid momentum theorem, the load

torque acting on the rotary valve can be determined as follow [19]:

$$T = \rho v_R^2 S_v R_0 \tag{4}$$

where T is the load torque acting on the rotary valve; ρ is the density of the fluid; v_R is the relative speed between the flow speed of the fluid and the rotation speed of the rotary valve; S_v is the effective area on the rotary valve, which is vertical to the direction of the flow speed; R_0 is the radius of the center of the effective area.

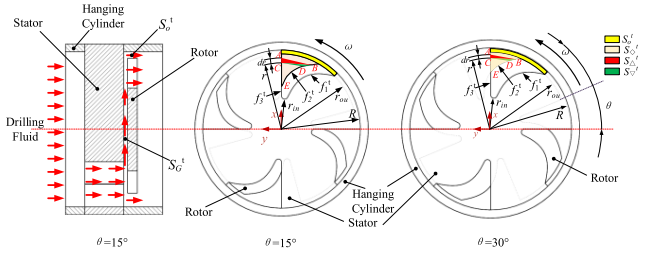

FIGURE 2. The flow area of each part in different rotation angle θ.

Through equation (4), it is obvious that the effective area and the properties of the drilling fluid have the main influence on the load torque, thus, it is necessary to determine the effective area firstly. The structure of the rotary valve is shown in Fig.2. In this figure, $\overrightarrow{f_1^t}$ is the curved edge of the stator at time t, $\overrightarrow{f_2^t}$ is the curved edge of the rotor at time t, $\overrightarrow{f_3^t}$ is the straight edge of the stator at time t and $\overrightarrow{f_i^t} \in \mathbb{R}^3 (i = 1, 2, 3)$. The X-axis coincides with the straight side of the stator $\overrightarrow{f_3^t}$. The relationship between these three curves can be described as follows:

$$\overrightarrow{f_2^t} = \overrightarrow{f_1^t} + \overrightarrow{s}^T \tag{5}$$

$$\overrightarrow{f_3^t} = \left\| \overrightarrow{f_1^t} \right\|_2 \overrightarrow{A}^T \tag{6}$$

where $\overrightarrow{s}$ represents the axial length of the gap and $\overrightarrow{s} = \begin{bmatrix} 0 & 0 & -s \end{bmatrix}$. $\overrightarrow{A}$ is the identical vector and $\overrightarrow{A} = \begin{bmatrix} 1 & 0 & 0 \end{bmatrix}$.

The valve is fully open when the rotation angle θ is 0. Moreover, when the rotation angle is θ, the throttle with a 3D variable cross-section shape is formed by the orifice curve $\overrightarrow{f_3^t}$ of the stator and the orifice curve $\overrightarrow{f_2^t}$ of the rotor. When the rotation angle is θ, the orifice curve $\overrightarrow{f_2^t}$ of the rotor can be determined as follow:

$$\overrightarrow{f_2^t} = \overrightarrow{f_2^0} Rot(\overrightarrow{\theta}) \tag{7}$$

where $\overrightarrow{f_2^0}$ means the orifice curve $\overrightarrow{f_2^t}$ of the rotor at $t = 0$;$Rot(\overrightarrow{\theta})$ is the coordinate transformation matrix and $Rot(\overrightarrow{\theta}) = \begin{pmatrix} \cos\left|\overrightarrow{\theta}\right| & \sin\left|\overrightarrow{\theta}\right| & 0 \\ -\sin\left|\overrightarrow{\theta}\right| & \cos\left|\overrightarrow{\theta}\right| & 0 \\ 0 & 0 & 1 \end{pmatrix}$; The rotation angle θ can be determined as $\overrightarrow{\theta} = \overrightarrow{\omega} t$ and $\overrightarrow{\omega}$ is the rotation speed of the rotor.

From Fig. 2, it can be found that the flow area can be divided into three parts and these three parts satisfy the following equation:

$$S^t = \sum \left| \overrightarrow{S_i^t} \right| (i = \diamondsuit, o, G) \tag{8}$$

where S^t is the total flow area at different time; $\overrightarrow{S_\diamondsuit^t}$ is the area vector of the curve flow area at time t, which is formed by the orifice curve $\overrightarrow{f_2^t}$ of the rotor and the orifice curve $\overrightarrow{f_3^t}$ of the stator; $\overrightarrow{S_o^t}$ is the area vector of the radial flow area formed by the rotor and the hanging cylinder; $\overrightarrow{S_G^t}$ is the area vector of the axial flow area at different time, which is formed by the gap.

Because of the irregular orifices, it is difficult to calculate the area vector of the curve flow area $\overrightarrow{S_\diamondsuit^t}$, thus, the finite element theory is used to discretize the curve flow area, then the area vector of the curve flow area $\overrightarrow{S_\diamondsuit^t}$ and the effective area of this part can be determined. As shown in Fig.2, the curve flow area $\overrightarrow{S_\diamondsuit^t}$ is differentiated into serval parts along the radial direction. The arcs at the radii r and $r+dr$ are intersected with the curves $\overrightarrow{f_2^t}$ and $\overrightarrow{f_3^t}$ at four points, A, B, C and D. When the rotation angle is θ, the curves $\overrightarrow{f_2^t}$ and $\overrightarrow{f_3^t}$ intersect at E. The two triangles CBA and BCD, formed by these four points, can approximate the area differential of the curve flow area $\overrightarrow{S_\diamondsuit^t}$. Using $\overrightarrow{S_\Delta^t}$ and $\overrightarrow{S_\nabla^t}$ to represent the area vector of CBA and BCD, and they can be calculated as follows:

$$\begin{aligned}
\overrightarrow{S_\diamondsuit^t} &= \sum_{j=\Delta}^{\nabla} N \int_{r_e}^{r_{ou}} \overrightarrow{S_j^t}\, dr \\
&= N \int_{r_e}^{r_{ou}} \left\{ \frac{1}{2} [\overrightarrow{f_3^t}(r) - \overrightarrow{f_2^t}(r + \mathrm{d}r)] \right. \\
&\quad \left. \times [\overrightarrow{f_3^t}(r + dr) - \overrightarrow{f_2^t}(r + \mathrm{d}r)] \right\} dr \\
&\quad + N \int_{r_e}^{r_{ou}} \left\{ \frac{1}{2} [\overrightarrow{f_2^t}(r + \mathrm{d}r) - \overrightarrow{f_3^t}(r)] \right. \\
&\quad \left. \times [\overrightarrow{f_2^t}(r) - \overrightarrow{f_3^t}(r)] \right\} dr \\
&= \frac{N}{2} \int_{r_e}^{r_{ou}} \left[\overrightarrow{f_3^t}(r) - \overrightarrow{f_2^t}(r + \mathrm{d}r) \right] \\
&\quad \times \left\{ \left[\overrightarrow{f_3^t}(r + dr) + \overrightarrow{f_3^t}(r) \right] - \left[\overrightarrow{f_2^t}(r + dr) + \overrightarrow{f_2^t}(r) \right] \right\} dr
\end{aligned} \tag{9}$$

where '×' indicates cross symbol, $\overrightarrow{S_\Delta^t}$ is the area vector of ΔCBA, $\overrightarrow{S_\nabla^t}$ is the area vector of ΔBCD, r_e is the polar radius of the point E, r_{ou} is the outer radius of the rotor.

To calculate the effective area of this part, the unit normal vectors $n_j (j = \Delta, \nabla)$ of $\overrightarrow{S_\Delta^t}$ and $\overrightarrow{S_\nabla^t}$ are firstly represented as

$$\overrightarrow{n_j} = \frac{\overrightarrow{S_j}}{|\overrightarrow{S_j}|} \tag{10}$$

At the single orifice, the area projection of ΔCBA and ΔBCD in the circumferential direction of the rotor can be

expressed as

$$\overrightarrow{S_{Cj}^t}(r) = |\overrightarrow{S_j^t}(r)|[\overrightarrow{n_j}(r) \cdot \overrightarrow{n_C}(r)] \tag{11}$$

where, $\overrightarrow{S_{c\Delta}^t}$ is the area projection of ΔCBA, $\overrightarrow{S_{c\nabla}^t}$ is the area projection of ΔBCD, and $\overrightarrow{n_c}(r)$ indicates the unit vector of the circumferential direction at the center points $\left[\overrightarrow{f_2^t}(r) + \overrightarrow{f_1^t}(r+dr)\right]/2$ of ΔCBA and ΔBCD.

The effective area $\overrightarrow{S_{eff}^t}$ of the curve flow area can be expressed as:

$$\overrightarrow{S_{eff}^t} = \int_{r_e}^{r_{ou}} \left(\sum \overrightarrow{S_{Cj}^t}(r)\right) dr \tag{12}$$

The radial flow area $\overrightarrow{S_o^t}$ is formed by the rotor and the hanging cylinder(shown in yellow in Fig.2), thus, it can be expressed as:

$$\left|\overrightarrow{S_O^t}\right| = \frac{1}{2}\left\{\pi R^2 - N[\theta + \sin(\frac{\pi}{N} - \theta)]r_{ou}^2\right\} \tag{13}$$

where R is the inner radius of the hanging cylinder.

For the axial flow area $\overrightarrow{S_G^t}$, when $t = 0$, the rotation angle is 0 and all the drilling fluid flows through the curve flow area and the radial flow area. With the rotation of the rotor, some drilling fluid flows through the gap because of the block of the rotor, and when the rotary valve is closed, almost all the drilling fluid flow through the gap and radial flow area. Therefore, the axial flow area is relative to the initial flow area and the initial flow area is formed by the curve flow area and the radial flow area when the rotation angle is 0. The initial flow area can be described as:

$$S_{Ini} = \left|\overrightarrow{S_\diamond^0}\right| + \left|\overrightarrow{S_o^0}\right| \tag{14}$$

where S_{Ini} is the initial flow area.

With the rotation of the rotor, some drilling fluid flowing through the gap is in a transition state. And this will cause not all drilling fluid to flow from the axial flow area. Thus, the flowing coefficient is defined to describe this phenomenon and the flowing coefficient can be described as follows:

$$w(x) = \frac{S_{Ini} - \left|\overrightarrow{S_\diamond^t}\right| - \left|\overrightarrow{S_o^t}\right|}{S_{Ini}} \tag{15}$$

where $w(x)$ is the flowing coefficient.

The axial flow area can be expressed as:

$$\begin{aligned}\overrightarrow{S_G^t} &= \overrightarrow{S_{str}^t} + \overrightarrow{S_{cur}^t} \\ &= -Nw(x)\int_{r_{in}}^{r_{ou}} \left[\overrightarrow{f_3^t}(r+dr) - \overrightarrow{f_3^t}(r)\right] \times \overrightarrow{s}\, dr \\ &\quad + Nw(x)\int_{r_{in}}^{r_e} \left[\overrightarrow{f_1^t}(r+dr) - \overrightarrow{f_1^t}(r)\right] \times \overrightarrow{s}\, dr\end{aligned} \tag{16}$$

where r_{in} is the inner radius of the rotor. Through Eqn.(1)$\sim$(16), the total effective flow area can be determined.

According to the fluid momentum theorem, the curve torque $\overrightarrow{T_\diamond}$ can be expressed as

$$\overrightarrow{T_\diamond} = N\rho \int_{r_e}^{r_{ou}} (\overrightarrow{v} + \overrightarrow{\omega} r)^2 r \left(\sum \overrightarrow{S_{Cj}^t}(r)\right) dr \tag{17}$$

where $\overrightarrow{v}$ is the flow velocity which can be expressed as $|\overrightarrow{v}| = Q/\left(\left|\overrightarrow{S_o^t}\right| + \left|\overrightarrow{S_G^t}\right| + \left|\overrightarrow{S_\diamond^t}\right|\right)$, its direction is in accordance with the normal direction of the flow area; $\overrightarrow{\omega}$ is the rotation speed of the rotor.

The flow area $\overrightarrow{S_o^t}$ is part of the total throttle area, so it will affect the flow velocity $\overrightarrow{v}$. As its flow direction is along in the Z-axis is consistent with the flow direction of the drilling fluid. Thus, the radial flow torque is 0. And the axial gap torque $\overrightarrow{T_G}$ can be described as follow:

$$\overrightarrow{T_G}(r) = N\rho \int_{r_{in}}^{r_{ou}} (\overrightarrow{v} + \overrightarrow{\omega} r) r d\overrightarrow{S_G^t} dr \tag{18}$$

Therefore, the total torque acting the rotor can be obtained as following:

$$\overrightarrow{T_s} = \overrightarrow{T_\diamond} + \overrightarrow{T_G} \tag{19}$$

According to the structure parameters of the rotary valve, drilling fluid density, drilling fluid flow rate, etc., the load torque acting on the rotary valve can be calculated by Equation (19).

III. CFD SIMULATION

A. MESH MODEL

To calculate the total load torque and save the experiment cost, the three-dimensional model of rotary valve the grid model is established as shown in Fig.3 and the parameters of the rotary valve model are shown in Table 1. According to these five parameters, the structure of rotary valve can be determined and used in the simulation to acquire the total load torque acting on the rotary valve. The valve model consists of five parts including the upstream flow, stator, rotor, gap and the downstream flow. In the mesh model, hexa meshes are used in all the regions, and the grids at the stator, rotor and gap are refined.

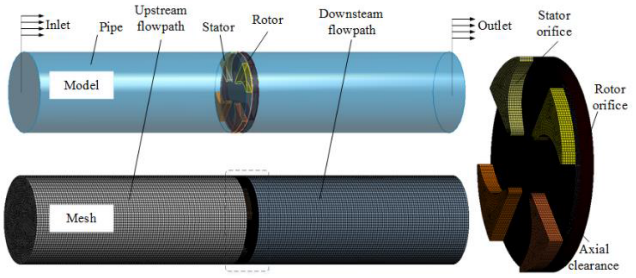

FIGURE 3. The mesh model of the rotary valve.

In the grid model, the initial rotation angle of the rotor is 0°. In the coordinate system, the Z-axis is the rotation axis. In the simulation, the surface of the rotor that revolves around the

TABLE 1. Design parameters.

SYMBOL	QUANTITY	VALUE
n	Blade number	4
R	Hanging cylinder radius	43mm
r_{ou}	Rotor radius	41mm
s	Clearance	2mm
ω	rotation speed	30r/min

TABLE 2. Mesh sizes in each location.

Location	Upstream	Stator orifice	Rotor orifice	Gap	Downstream
Nodes	107996	17136	112619	995661	107996
Elements	101559	13560	96456	882776	101559
Element Size (mm)	2.5	1.0	0.5	0.25	2.5

Z-axis is set as a wall. And a monitor is set to acquire the load torque acting on the wall. The mesh sizes used in the simulation are shown in Table 2.

B. TURBULENCE MODEL

Due to the flow speed of drilling fluid flowing through the valve orifices is very high, the fluid flow at the rotary valve should normally be turbulent. Among similar simulation problems, $k-\varepsilon$ model is widely used for some valves and has achieved good results, such as safety relief valve [26], globe valve [27] and logic valve [28], and also the rotary valve [19]. Therefore, the section will also choose $k-\varepsilon$ model to solve load torque acting on rotary valve with irregular valve port. $k-\varepsilon$ model can be described as following [29]:

$$\frac{\partial(\rho k)}{\partial t}+\nabla\cdot(\rho\vec{u}\,k)=\nabla\cdot((\mu+\frac{\mu_t}{\sigma_k})\nabla k)+2\mu_t S_{ij}\cdot S_{ij}-\rho\varepsilon \tag{20}$$

$$\frac{\partial(\rho\varepsilon)}{\partial t}+\nabla\cdot(\rho\vec{u}\,\varepsilon)=\nabla\cdot((\mu+\frac{\mu_t}{\sigma_\varepsilon})\nabla k)+2C_{1\varepsilon}\frac{\varepsilon}{k}\mu_t S_{ij}\cdot S_{ij}-C_{2\varepsilon}\rho\rho\frac{\varepsilon^2}{k} \tag{21}$$

Turbulent viscosity μ_t can be calculated as following:

$$\mu_t=C_\mu\rho\frac{k^2}{\varepsilon} \tag{22}$$

where u is the flow velocity, μ is the kinematic viscosity, and S_{ij} is the average component of the deformation rate of the fluid elements in the turbulent flow. In the standard k $-$ ε model $C_{1\varepsilon}=1.44, C_{2\varepsilon}=1.92, C_\mu=0.09$, $\sigma_k=1.00, \sigma_\varepsilon=1.30$.

C. BOUNDARY CONDITIONS AND SOLVING METHOD

From Fig. 3, the outlet type is set to a constant pressure outlet with a relative pressure of 0MPa. To analyze the load torque acting on the rotor under different flow rates, the inlet type is set to the speed inlet. The domain at the rotor is set to a rotating domain. During the simulation, the moving mesh is used in the rotation domain and the mesh in the rotating domain will rotate to simulate the rotation of the rotor. All wall boundaries are assumed to be non-slip boundaries and satisfy the standard wall equations in the near wall area.

In the simulation, the density of mud is 997 kg/m^3 and the dynamic viscosity is 8.9×10^{-5}kg/(m·s). For the scaling residuals of all parameters, the absolute standard of convergence is set to 10^{-4}. There are some assumptions in the simulation: incompressible liquid, ignoring leaks and channel wall roughness, constant liquid properties, and thermal equilibrium conditions.

IV. EXPERIMENT

To verify the correctness of the theoretical model, a rotary valve is firstly designed based on the method proposed in [7] and used in the experiment. To show the structure and shape of the rotary valve clearly, the physical model is illustrated in Fig.4 and the key parameters are shown in Table 1. The rotary valve consists of a pair of stator and rotor that contain four blades with the same shape. The sizes of the stator and rotor are shown in Table 1.

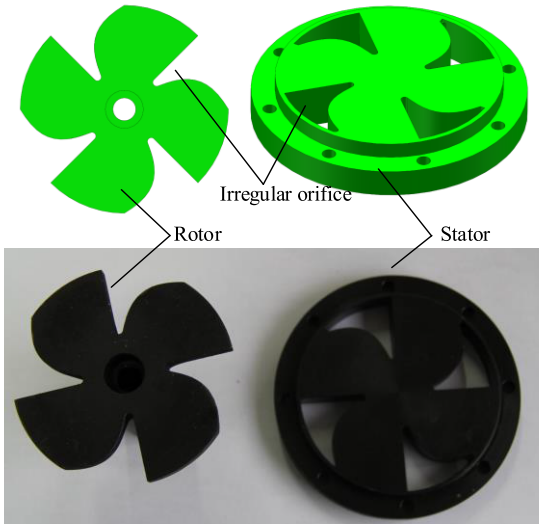

FIGURE 4. CAD model and prototype of the rotary valve structure.

The rotary valve test system is shown in Fig. 5. The rotary valve is mounted in a test equipment that can use its own flowmeter to measure the flow rates through the valve and display it on the display screen. The rotor driven by a servo motor rotates continuously. The rotation angle of the rotor can be monitored by an angle encoder in real time. At the same time, the load torque will be measured by a torque sensor installed between the servo motor and the angle encoder. The load torque and angle information can be collected and transferred to a computer by a signal acquisition device. The mud pump is a triplex reciprocating pump that can output an approximate constant flow rate, and the adjustable throttle valve is amounted at the outlet of the circulating pipeline to

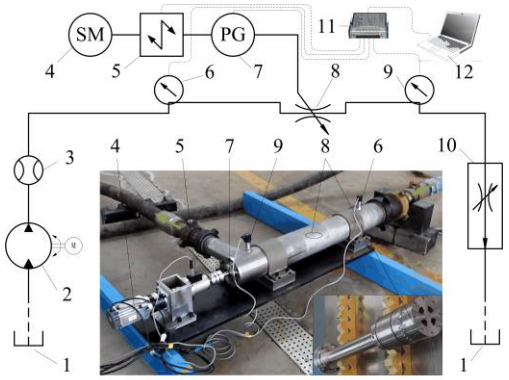

FIGURE 5. The rotary valve test system:1-water tank, 2-mud pump, 3-flowmeter, 4-servo motor, 5-torque sensor, 6-inlet pressure sensor, 7-angle encoder, 8-rotary valve, 9-outlet pressure sensor, 10-throttle valve, 11- signal acquisition device, 12-computer.

avoid a vacuum at the outlet of the valve when the valve is closed.

In actual drilling operations, the discharge of the drilling fluid is in the range of 10L/s to 35L/s. And this method is suitable for use in water-based drilling fluids or oil-based drilling fluids, at the same time, the influencing law is unchanged when the drilling fluid or water is used. Therefore, based on laboratory conditions, water is used instead of the drilling fluid. In the experiment, the flow rate of the water in the system is set to 20 L/s by adjusting the output of the pump. Because the theory model can calculate the load torque at any rotation speed, to measure the load torque more accurately, the rotation speed is chosen as 30r/min, thus, the frequency of the generated continuous wave is 2Hz as there are four orifices [2]. The values measured by the torque sensor include the load torque acting on the rotor and the system friction torque, such as the friction torque of the rotating seal and bearing. Thus, in the experiment, the rotary valve is taken off and the drilling fluid with different pressure is pumped into the pipe. Then the servo motor rotates at different speed and the friction torque can be measured. As shown in Table 3, there is a large friction torque, and the friction torque acting on the system decreases as the rotation speed increases and increases as drilling fluid pressure increases. According to the experimental conditions, the friction torque of 1.3Nm is chosen at the rotation speed of 30 r/min and the pressure of 2MPa.

TABLE 3. Friction torque at the discharge of 20L/s.

TORQUE ($N \cdot m$)	DRILLING FLUID PRESSURE			
Rotation speed	0MPa	1MPa	1.5MPa	2MPa
7.5r/min	1.3	1.5	1.9	2
15r/min	1	1.3	1.6	1.8
30r/min	1	1	1.3	1.3

The total torque measured by the sensor in the experiment is shown in Fig. 6, and there is high frequency noise and the friction torque with 1.3Nm in the torque signal. The high

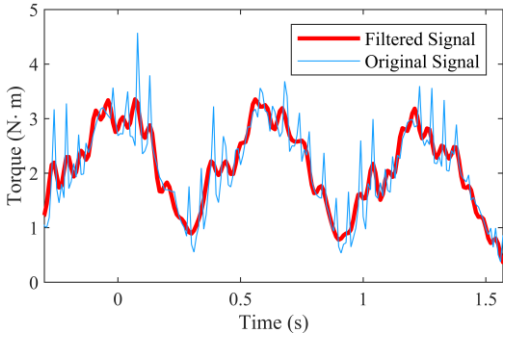

FIGURE 6. The measured load torque.

frequency noise is removed using a low pass filter with cut-off frequency of 5Hz, the friction torque of 1.3Nm is subtracted, and then the flow torque acting on the rotary valve will be obtained as shown in Fig. 6.

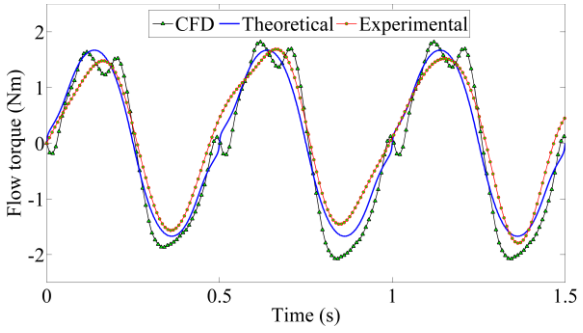

FIGURE 7. Comparison of simulation torque, theoretical torque and experimental torque.

TABLE 4. Difference of theoretical calculation and experimental test based on CFD simulation results.

Error (%)	Theoretical calculation	Experiment
Maximum Error	22.3	30.1
Minimum Error	1.28	2.8

V. RESULT AND DISCUSSION

Theoretical calculations, CFD simulation and experimental results from which the noise and friction torque are removed are shown in Fig. 7. The error of theoretical calculation and experiment is shown in Table 4. It can be seen from the table and figure that the theoretical value is close to the simulated value (the maximum error is about 22.3% and the minimum error is about 1.28%). The error may be caused by the assumptions in the theoretical calculation. For example, the turbulence is also not considered in the theoretical model, and there is no consideration of the phenomenon of swirl when the rotor rotates. The experimental value is slightly larger than the theoretical value, but the trend of change is

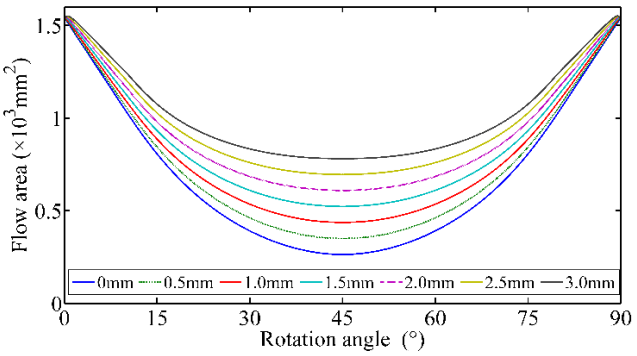

FIGURE 8. The change of the curve $\left|\overrightarrow{S_{\diamond}^{t}}\right|$ flow area with the rotation angle under different gaps.

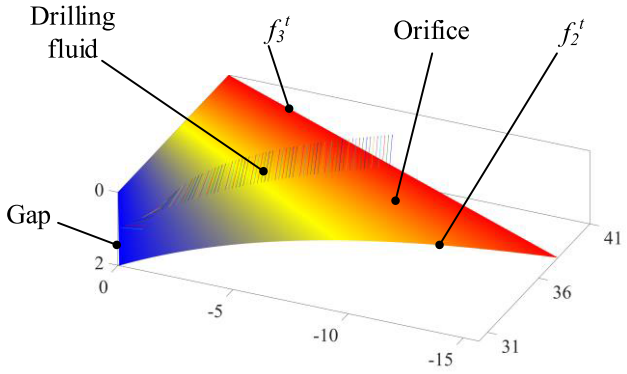

FIGURE 9. The flow chart of the fluid with the clearance of 2mm and the angle of 22.5°.

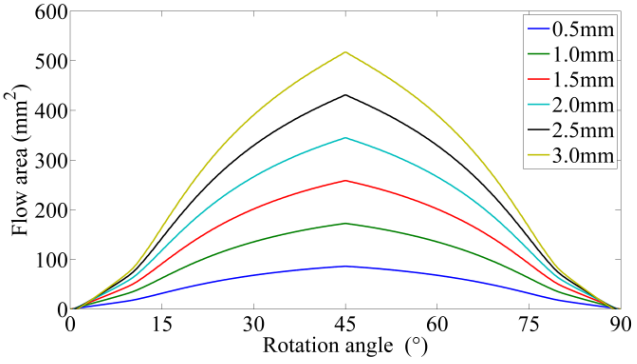

FIGURE 10. The axial flow area $\left|\overrightarrow{S_{G}^{t}}\right|$ changing with the rotation angle under different gaps.

same (the maximum error is about 30.1% and the minimum error is about 2.8%). This error can be caused by frictional disturbances, pressure fluctuations and measurement errors, etc. Besides, there is a certain difference between the physical and theoretical models of the rotary valve due to the influence of machining error and assembly error, which will also lead to a deviation between the experimental results and the theoretical results. Approximately, theoretical calculations and CFD simulations can be validated by the experimental result, so the proposed theory model can be used to predict the load torque acting on the rotary valve with the irregular orifices.

Based on the proposed theoretical model, the influence factors of load torque are analyzed. As shown in Fig. 8, it is obvious that as the gap size increases, the minimum curve flow area $\left|\overrightarrow{S_{\diamond}^{t}}\right|$ becomes larger. When the gap is constant, the curve flow area $\left|\overrightarrow{S_{\diamond}^{t}}\right|$ firstly decreases and then increases with the rotation of the rotor, and the flow area $\left|\overrightarrow{S_{\diamond}^{t}}\right|$ is minimum when the rotation angle is 45°. With the rotation of the rotor, the area where the stator and rotor overlap is gradually increased. And it will cause point E to gradually approach the outer edge of the rotor. When the rotation angle is 45°, the polar radius r_e is nearly equal to the outer radius r_{ou}. Therefore, the curve flow area $\left|\overrightarrow{S_{\diamond}^{t}}\right|$ gradually decreases when the rotation angle is less than 45° and is minimum when the rotation angle is 45°. According to the previous research, when the flow rate is constant, the greater minimum flow area will lead to the smaller amplitude of the pressure wave. Thus, it can be concluded that different gap will lead to different amplitude of the pressure wave. In the actual drilling engineering, the optimum gap can be determined according to the demand amplitude of pressure wave, and then the curve torque $\overrightarrow{T_{\diamond}}$ can be determined.

When the gap size is 2mm and the rotation angle is 22.5°, the shape of the orifice formed by the rotor and stator is shown in Fig.9. It can be found that the orifice formed by $\overrightarrow{f_2^t}$ and $\overrightarrow{f_3^t}$ is irregular, and the flow direction is not the same at different locations. It also shows that with the different polar radius r, the normal directions of $\overrightarrow{S_{\Delta}^{t}}$ and $\overrightarrow{S_{\nabla}^{t}}$ are different.

Combining with Fig.8, it can analyze the changing law of the curve flow area $\overrightarrow{S_{\diamond}^{t}}$ with the rotation angle under different gaps. From this result, it can be concluded that the change of the flow direction will lead to different curve torque $\overrightarrow{T_{\diamond}}$. In the previous research, the orifice is simple rectangular, and the jet direction of the fluid is same along the curve of the valve port. Thus, it is difficult to use the previous model to describe the characteristics of the load torque acting on the rotary valve with irregular orifices, and our model can solve these two types of problems well.

The relationship between the axial flow area $\left|\overrightarrow{S_{G}^{t}}\right|$ and the rotation angle θ is shown in Fig. 10. From this figure, with the rotation angle increases, the flow area $\left|\overrightarrow{S_{G}^{t}}\right|$ firstly increases and then decreases, which is opposite to the changing law of the curve flow area $\left|\overrightarrow{S_{\diamond}^{t}}\right|$. The bigger gap means the larger minimum flow area $\left|\overrightarrow{S_{G}^{t}}\right|$, and the flow area $\left|\overrightarrow{S_{G}^{t}}\right|$ reaches the maximum value when the rotation angle is 45°. According to the mathematic model, with the rotation of the rotor, $\overrightarrow{S_{cur}^{t}}$ and $w(x)$ increase, which means more drilling fluid flows through the gap formed by $\overrightarrow{f_1^t}$ and the rotor. At the same time, the increasing $w(x)$ means less drilling fluid is in the transition state.

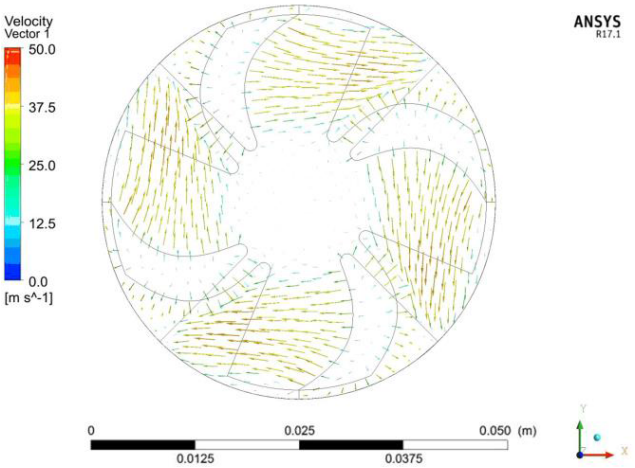

FIGURE 11. Flow velocity vector at the gap of 2mm and the rotation angle of 22.5°.

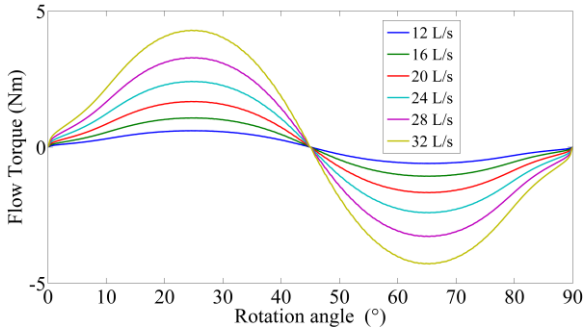

FIGURE 12. Change of the load torque T_t with rotation angle under different flow rate.

According to CFD analysis, the flow velocity vector at the gap is shown in Fig. 11. At this point, the gap size is 2mm and the rotation angle is 45°, the flow area formed by the gap is the largest, and drilling fluid mainly flows along the circumferential direction. The flow velocity is up to 40m/s. The result can explain that the assumptions about flow velocity $\overrightarrow{v}$ is reasonable. Combination with Fig.8 and Fig. 10, it is obvious that the gap size has a great influence on the flow torque acting on the rotor.

When the gap size is 2mm and the rotation speed is 0.5r/min, the relationship between the load torque and the flow rate is shown in Fig.12. It is obvious that the load torque presents a periodic change as the rotation angle increase, and the curve is centrally symmetric at the 45° position. With the increase of the flow rate, the maximum load torque becomes larger, and the maximum values are all reached at a certain angle.

When the rotation angle is 45°, the curve flow area $\left|\overrightarrow{S_\diamond}\right|$ reaches the minimum value while the axial flow area $\left|\overrightarrow{S_G}\right|$ is maximum. The curve torque $\overrightarrow{T_\diamond}$ is nearly equal to 0, at the same time, the direction of $\overrightarrow{S_{str}^t}$ and $\overrightarrow{S_{cur}^t}$ is opposite, which

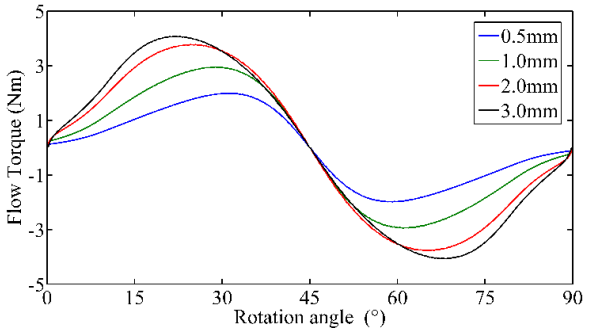

FIGURE 13. Change of load torque with angle under different gap sizes.

will lead to the nearly zero load torque $\overrightarrow{T_t}$. When the rotation angle is between 0 and 45°, because of the change of the curve torque $\overrightarrow{T_\diamond}$ and the torque caused by $\overrightarrow{S_{cur}^t}$, the load torque T_t fluctuates with the rotation angle. With the discharge increasing, more drilling fluid flows through the rotary valve and the unchanged structure will lead to the same $\overrightarrow{S_\diamond}$ and $\overrightarrow{S_G}$ in the same rotation angle. It will lead to the larger flow velocity v, and the load torque is proportional to the flow velocity v. As the result, the load torque increases with the discharge.

The load torque curves in different gap sizes are shown in Fig.13. It is obvious that with the increase of the gap size, the amplitudes of the load torque become larger and the rotation angle where the load torque reaches the maximum value increases. According to the mathematic model, with the increasing of the gap size, the axial flow area $\left|\overrightarrow{S_G^t}\right|$ becomes larger, which will lead to the increase of the $\left|\overrightarrow{T_G}\right|$. At the same time, based on the assumption of incompressible fluid, the discharge flowing through the curve flow area $S_\diamond$ is unchanged, and in the same rotation angle, the curve flow area $\left|\overrightarrow{S_\diamond^t}\right|$ is also unchanged, which means the curve flow torque is the same and the amplitudes of the load torque increase with the increasing gap sizes.

With the increase of the gap size, the axial flow area $\left|\overrightarrow{S_G^t}\right|$ becomes larger and the curve flow area $\left|\overrightarrow{S_\diamond^t}\right|$ decreases and more drilling fluid flows through the axial flow area $\left|\overrightarrow{S_G^t}\right|$. When compared to the curve flow area $\left|\overrightarrow{S_\diamond}\right|$, the axial flow area $\left|\overrightarrow{S_G}\right|$ cannot be neglected, the total load torque reaches the maximum value. Thus, with the gap size increasing, the rotation angle where the total load torque reaches the maximum value decreases. According to the analysis result, in actual rotary valve design, we should try to avoid changing the gap size. There are also some assumptions: hypothetical spacing in theoretical model is far less than the size of valve and each unit of fluid is independent and does not affect each other.

As shown in Fig. 14, the real line describes the size of the total torque, and the dotted line describes the load torque produced by the fluid over the gap. With the rotation of the rotor,

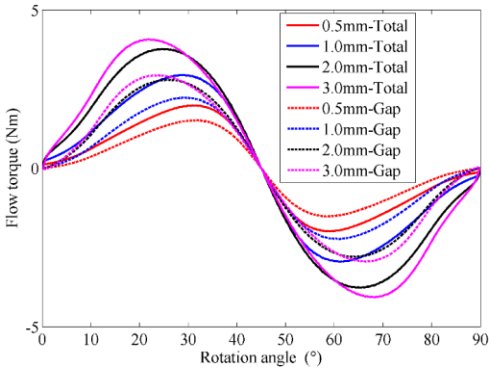

FIGURE 14. The total flow torque and flow torque effected by the gap under different gap sizes.

the proportion of torque acting on the rotor flowing through the axial gap firstly increases to 99%, and then decreases gradually and finally stabilizes at 23 %. The percentage of torque flowing through the shape of the valve port firstly decreases to 1% with the increase of the rotation angle of the rotor, gradually increases, and finally stabilizes at 77%. With the gap size increasing, the proportion of torque acting on the rotor flowing through the axial gap becomes less. It is obvious that when the rotation angle changes in 0° to 22.5°, more and more torques are created by the fluid that flows over the gap.

Through the analysis of the above figure, the theoretical model can describe the load torque acting on the rotary valve with irregular valve shape. The load torque is symmetrical at the location of 45° and has obvious characteristics with the change of flow rate, clearance and rotation angle. This change trend provides theoretical guidance for the actual rotary valve design.

VI. CONCLUSION

In this paper, a method of calculating the load torque acting on the rotary valve with the irregular orifice is proposed, and the mathematic model describing the load torque is established and verified by the CFD simulation and the experiment. The following conclusions are obtained:

(1) The theoretical model is verified by the CFD and experiment, and the mathematic model can be used to calculate the load torque acting on the rotary valve and analyze the changing laws of the load torque.

(2) The magnitude and trend of the load torque are affected by flow rate, gap size and orifice area. And the load torque is symmetrical at the location of 45°. The change of flow rate will lead to the increase of the maximum value of the load torque and the change of gap size will change the maximum load torque and the rotation angle where the load torque reaches the maximum value. When the rotation angle is between 0 and 45°, the curve flow area decreases with the increasing rotation angle while the axial flow torque increases.

(3) The direction of the load torque is always the direction the valve wants to be closed. As the orifice increases, the torque acts as a resistance to rotor rotation and serves to push the rotor to turn as the orifice opening decreases. The axial flow area occupies a large proportion in the total flow area of the rotary valve, and has a great influence on the load torque of the rotary valve.

(4) Due to the alternation and high amplitude of the load torque, it is difficult to use the ordinary control strategy to control the DFCW generator to generate the specific waveform. Therefore, it is necessary to design the suitable control strategy and chose the suitable motor to achieve the servo control with high performance with high and alternating load torque.

(5) In the theoretical model, the flow state is considered as laminar flow, and the influence of solid in the drilling fluid is neglected. And it should be studied in the future research.

ACKNOWLEDGMENT

The authors would like to thank the anonymous reviewers for their valuable suggestions and corrections.

REFERENCES

[1] C. Zhang, H. Dong, J. Wang, J. Ge, H. Liu, Z. Yuan, J. Zhu, and H. Zhang, "A low error rate BCH-based encoder-decoder approach for electromagnetic measurement while drilling system," *IEEE Access*, vol. 7, pp. 34599–34608, 2019.

[2] J. Wu, B. Zhou, D. Qin, and R. Wang, "Mathematical model and analysis of characteristics of downhole continuous pressure wave signal," *J. Petroleum Sci. Eng.*, vol. 186, Mar. 2020, Art. no. 106706.

[3] C. Klotz, I. Wassermann, and D. Hahn, "Highly flexible mud-pulse telemetry: A new system," in *Proc. SPE Indian Oil Gas Tech. Conf. Exhib./ Soc. Petroleum Eng.*, 2008.

[4] A. Caruzo, R. Hutin, S. Reyes, A. Tweel, and P. Temple, "Advanced design and execution techniques for delivering high data rate MWD telemetry for ultradeep wells," in *Proc. OTC Arctic Technol. Conf.*, 2012.

[5] R. Hutin, R. W. Tennent, and S. V. Kashikar, "New mud pulse telemetry techniques for deepwater applications and improved real-time data capabilities," in *Proc. SPE/IADC Drilling Conf./ Soc. Petroleum Eng.*, 2001.

[6] C. Klotz, P. R. Bond, I. Wassermann, and S. Priegnitz, "A new mud pulse telemetry system for enhanced MWD/LWD applications," in *Proc. IADC/SPE Drilling Conf./ Soc. Petroleum Eng.*, 2008.

[7] J. Wu, R. Zhang, and R. Wang, "Mathematical model and optimum design approach of sinusoidal pressure wave generator for downhole drilling tool," *Appl. Math. Model.*, vol. 47, pp. 587–599, Jul. 2017.

[8] D. Hahn, V. Peters, C. Rouatbi, and H. Eggers, "Oscillating shear valve for mud pulse telemetry and associated methods of use," U.S. Patent 6 975 244, Dec. 13, 2005.

[9] E. Lavrut, A. Kante, P. Rellinger, and S. R. Gomez, "Pressure pulse generator for downhole tool," U.S. Patent 6 970 398, Nov. 29, 2005.

[10] K. A. Moriarty, "Method and system for wellbore communication," U.S. Patent 7 552 761, Jun. 30, 2011.

[11] C. A. Perry, D. E. Burgess, and W. E. Turner, "Rotary pulser for transmitting information to the surface from a drill string down hole in a well," U.S. Patent 7 327 634, Feb. 5, 2008.

[12] P. Jia, "Design of drilling fluid continuous wave generator and experiment research of signal transmission characteristic," M.S. thesis, School Mech. Eng., China Univ. Petroleum, Qing Dao, China, 2010.

[13] Z. Yan, Y. Geng, C. Wei, T. Wang, T. Gao, J. Shao, X. Hu, and M. Yuan, "Design of a continuous wave mud pulse generator for data transmission by fluid pressure fluctuation," *Flow Meas. Instrum.*, vol. 59, pp. 28–36, Mar. 2018.

[14] Y. Zhidan, W. Chunming, G. Yanfeng, S. Jing, H. Xiufeng, and L. Yuan, "Design of a rotary valve orifice for a continuous wave mud pulse generator," *Precis. Eng.*, vol. 41, pp. 111–118, Jul. 2015.

[15] M. A. Namuq, M. Reich, and S. Bernstein, "Continuous wavelet transformation: A novel approach for better detection of mud pulses," *J. Petroleum Sci. Eng.*, vol. 110, pp. 232–242, Oct. 2013.

[16] B. Zhou, J. Wu, M. Martin, and N. Han, "Design and analysis of motor control system for drilling fluid continuous wave generator based on improved active disturbance rejection control and hysteresis current control," in *Proc. Int. Conf. Intell. Robot. Appl.* Cham, Switzerland: Springer, 2019, pp. 569–579.

[17] Y. Yue, Y. Geng, W. Wang, K. Kim, Y. Xu, and Y. Yue, "A noval speed control strategy based on multi model framework for continuous wave mud pulser," in *Proc. Chin. Autom. Congr. (CAC)*, Oct. 2017, pp. 4119–4122.

[18] I. Okhotnikov, S. Noroozi, P. Sewell, and P. Godfrey, "Evaluation of steady flow torques and pressure losses in a rotary flow control valve by means of computational fluid dynamics," *Int. J. Heat Fluid Flow*, vol. 64, pp. 89–102, Apr. 2017.

[19] H. Wang, G. Gong, H. Zhou, and W. Wang, "Load torques in a servo motor operated rotary directional control valve," *Energy Convers. Manage.*, vol. 112, pp. 1–10, Mar. 2016.

[20] R. Amirante, G. D. Vescovo, and A. Lippolis, "Flow forces analysis of an open center hydraulic directional control valve sliding spool," *Energy Convers. Manage.*, vol. 47, no. 1, pp. 114–131, Jan. 2006.

[21] R. Amirante, G. Del Vescovo, and A. Lippolis, "Evaluation of the flow forces on an open centre directional control valve by means of a computational fluid dynamic analysis," *Energy Convers. Manage.*, vol. 47, nos. 13–14, pp. 1748–1760, Aug. 2006.

[22] P. Saravanakumar, K. K. Manesh, M. Singaperumal, and B. Ramamoorthy, "Modelling of fluid continuum considering 3D surface parameters in hydraulic assemblies," *Precis. Eng.*, vol. 33, no. 1, pp. 99–106, Jan. 2009.

[23] S. Yoshimoto, T. Shou, and K. Somaya, "Vertical attractive force generated in a noncontact chuck using ultrasonic vibration," *Precis. Eng.*, vol. 37, no. 4, pp. 805–811, Oct. 2013.

[24] P. Ranjan, R. Balasubramaniam, and V. K. Jain, "Analysis of magnetorheological fluid behavior in chemo-mechanical magnetorheological finishing (CMMRF) process," *Precis. Eng.*, vol. 49, pp. 122–135, Jul. 2017.

[25] H. Nouraei, K. Kowsari, M. Papini, and J. K. Spelt, "Operating parameters to minimize feature size in abrasive slurry jet micro-machining," *Precis. Eng.*, vol. 44, pp. 109–123, Apr. 2016.

[26] X. Song, L. Cui, M. Cao, W. Cao, Y. Park, and W. M. Dempster, "A CFD analysis of the dynamics of a direct-operated safety relief valve mounted on a pressure vessel," *Energy Convers. Manage.*, vol. 81, pp. 407–419, May 2014.

[27] J.-Y. Qian, L. Wei, Z.-J. Jin, J.-K. Wang, H. Zhang, and A.-L. Lu, "CFD analysis on the dynamic flow characteristics of the pilot-control globe valve," *Energy Convers. Manage.*, vol. 87, pp. 220–226, Nov. 2014.

[28] E. Lisowski, W. Czyżycki, and J. Rajda, "Multifunctional four-port directional control valve constructed from logic valves," *Energy Convers. Manage.*, vol. 87, pp. 905–913, Nov. 2014.

[29] H. K. Versteeg and W. Malalasekera, *An Introduction to Computational Fluid Dynamics*. Upper Saddle River, NJ, USA: Prentice-Hall, 2007.